International Journal of Disaster Risk Reduction 84 (2023) 103338

Contents lists available at ScienceDirect

International Journal of Disaster Risk Reduction

journal homepage: www.elsevier.com/locate/ijdrr

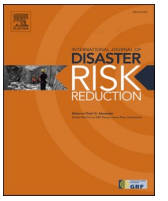

Physics-based simulations of multiple natural hazards for risk-sensitive planning and decision making in expanding urban regions

Luke T. Jenkins [a,*], Maggie J. Creed [b], Karim Tarbali [c], Manoranjan Muthusamy [d,e], Robert Šakić Trogrlić [f,g], Jeremy C. Phillips [a], C. Scott Watson [h], Hugh D. Sinclair [d], Carmine Galasso [i], John McCloskey [c]

[a] School of Earth Sciences, Wills Memorial Building, University of Bristol, Bristol, BS8 1RJ, UK
[b] James Watt School of Engineering, University of Glasgow, Glasgow, G12 8QQ, UK
[c] Grant Institute, School of GeoSciences, The University of Edinburgh, Edinburgh, EH9 3FE, UK
[d] School of GeoSciences, The University of Edinburgh, Edinburgh, EH8 9XP, UK
[e] FloodFlash, London, E1 8DN, UK
[f] Department of Geography, King's College London, London, WC2B 4BG, UK
[g] Systemic Risk and Resilience (SYRR) Group, Advancing Systems Analysis (ASA) Program, International Institute for Applied Systems Analysis (IIASA), Laxenburg, 2361, Austria
[h] COMET, School of Earth and Environment, University of Leeds, Leeds, LS2 9JT, UK
[i] Department of Civil, Environmental and Geomatic Engineering, University College London (UCL), London, WC1E 6BT, UK

ARTICLE INFO

Keywords:
Natural hazards
Physics-based modelling
Risk-sensitive urban planning

ABSTRACT

Rapid urban expansion in many parts of the world is leading to increased exposure to natural hazards, exacerbated by climate change. The use of physics-based models of natural hazards in risk-informed planning and decision-making frameworks may provide an improved understanding of site-specific hazard scenarios, allowing various decision makers to more accurately consider the consequences of their decisions on risks in future development. We present results of physics-based simulations of flood, earthquake, and debris flow scenarios in a virtual urban testbed. The effect of climate change, in terms of increasing rainfall intensity, is also incorporated into some of the considered hazard scenarios. We use our results to highlight the importance of using physics-based models applied to high-resolution urban plans to provide dynamic hazard information at the building level for different development options. Furthermore, our results demonstrate that including building elevations into digital elevation models is crucial for predicting the routing of hazardous flows through future urban landscapes. We show that simulations of multiple, independent hazards can assist with the identification of developing urban regions that are vulnerable to potential multi-hazard events. This information can direct further modelling to provide decision-makers with insights into potential multi-hazard events. Finally, we reflect on how information derived from physics-based hazard models can be effectively used in risk-sensitive planning and decision-making.

* Corresponding author.
E-mail address: luke.jenkins@bristol.ac.uk (L.T. Jenkins).

https://doi.org/10.1016/j.ijdrr.2022.103338
Received 14 May 2022; Received in revised form 28 September 2022; Accepted 29 September 2022
Available online 8 October 2022

1. Introduction

Urban areas are often hotspots of natural-hazard disaster risks due to their growing populations, ageing and inadequate infrastructure, rising inequality, rapid expansion, and poor spatial planning (e.g., [1]). For example, an analysis conducted by Gu [2] assessed exposure and vulnerability to six different natural hazards for 1860 cities with 300,000 inhabitants or more; 1087 of these cities have a high level of exposure to at least one natural hazard, and 45 cities are highly exposed to three or more natural hazards. Considering multiple hazards is crucial for urban development, as failing to do so can lead to underestimation of the overall impacts and associated risk (e.g., [3]). Multiple hazards should be considered from the spatial planning perspective when choosing suitable areas for development, as different hazards can affect different areas within an urban region (e.g., [4]). This includes both the expansion and renewal of an urban area, as both can provide an opportunity for reducing disaster risks and introducing new risks. Therefore, risk-informed planning and decision making is considered a prerequisite for safer and more resilient urban futures [5,6].

Modelling natural hazards can provide city planners, municipalities, and communities with information on potential hazard scenarios, enabling effective urban design and decision-making that can reduce physical, social, and economic disaster impacts in future urban settings. This information is often presented to stakeholders in the form of hazard maps that display quantitative estimates of susceptibility and/or site-specific intensities of future hazards, for example: landslide susceptibility; peak-ground acceleration or other ground-motion features (e.g., spectral acceleration, significant duration) from earthquakes; maximum flood depth or velocity and flood duration; thickness of volcanic ash deposits; peak wind speeds during storms. Hazard maps are useful for land-use planning and urban design, as they allow urban growth plans to account for threats posed by natural hazards (e.g., [7,8]). However, the use of hazard maps in risk-sensitive urban planning is typically limited to single hazards or multiple independent hazards that do not dynamically interact [9,10]. Yet, Global South cities, which account for most global urban growth (e.g., [11]), will continue to be disproportionally exposed and vulnerable to natural hazards and their interactions. Among other reasons, this is due to a lack of risk-sensitive urban planning (e.g., [5,6,12]). Therefore, integrating models of natural hazards within risk-sensitive urban planning and decision-making frameworks may effectively reduce disaster risk to vulnerable future communities (e.g., [89]; this special issue).

Hazard models can broadly be divided into two primary categories: physics-based and non-physical models, including empirical and stochastic methods (e.g., [13]). Understanding the advantages and limitations of these model types is crucial, allowing multiple stakeholders to gain the most appropriate information when designing and selecting risk-sensitive urban plans. Non-physical methods apply statistical approaches to observational datasets to estimate broad-scale features of natural hazards. For example, Rickenmann [14] compiles common empirical relationships between debris flow volume, peak discharge, mean flow velocity and run-out length. These models often have functional forms that are, even if in a simple manner, informed based on physical considerations. Although these and other empirical models are helpful in many applications of hazard assessment, non-physical models are limited when spatiotemporal hazard information on high-resolution urban topography is required. For example, an empirical description of flow inundation calibrated for a particular topography cannot reliably predict inundation where the flow is perturbed by interactions with buildings whose configuration can vary widely in different global cities and future urban layouts. For effective risk-sensitive planning of future urban environments, asset-scale (i.e., at the scale of individual buildings, bridges, roads and other infrastructure) information of hazard intensities and their physical/social impacts is required to reduce disaster risk and increase resilience. In this work, we define 'physics-based' models as methods that simulate the dynamics of natural-hazard events by solving partial differential equations (PDEs) that enforce physical conservation laws (e.g., energy, mass, momentum). Note that physics-based models often incorporate empirical relationships within the system of governing equations. Furthermore, empirical data is often used to prescribe poorly defined aspects of simulation domains. For example, empirical data can be used to define seismic velocity-depth relationships in the absence of a rigorous velocity model (see Section 3). Physics-based simulations can be applied to high-resolution topography to provide detailed information on hazards in time and space and account for interactions with the built environment on hazard propagation. One advantage of using physics-based models for assisting with future urban planning is that the parameters contained within these models have a physical meaning (e.g., slope angle, basal drag coefficient, rock density, etc.). Hence, changes to these physical parameters in future scenarios can be theoretically accounted for. Conversely, it is difficult to interpret the non-physical parameters that feature in empirical and stochastic models (e.g., [13]), and predict how these parameters will evolve with future urban development, climate change, and other processes.

Purely stochastic and empirical methods cannot typically provide accurate time-dependent information due to their simplification of the physical processes that control natural hazards. In addition, it is difficult to calibrate empirical and stochastic methods for the largest magnitude events due to their scarcity in historical records. For example, 'giant' earthquakes (moment magnitude, $M_w \geq 9$) can have a recurrence interval of hundreds to thousands of years (e.g., [15]), meaning that empirical ground-motion models (GMMs) are often calibrated with more frequent, small-to-moderate magnitude earthquakes better represented in empirical databases. This, combined with the simplified empirical representation of physical processes (e.g., fault rupture, seismic wave propagation/attenuation, near-surface soil response), limits the ability of GMMs to provide accurate hazard information that can allow cities to plan for the most hazardous earthquakes (e.g., [16]). Empirical and stochastic methods often require large quantities of site-specific data, meaning that they are typically less geographically transferable. This can also be a problem for some physics-based models sensitive to spatial parameter variations. For example, physics-based modelling of earthquake-induced ground motions requires location-specific velocity models of the subsurface. In contrast, empirical GMMs, in some instances, may be more transferable once calibrated for a specific region (e.g., [17]). Furthermore, empirical and stochastic methods are typically less suitable for urban planning, as data in undeveloped areas is often unavailable or poorly resolved in space and time.

Despite the various advantages discussed above, a critical limitation of physics-based models is that a degree of specialist knowledge is required to set up and calibrate physics-based hazard simulations. In addition, physics-based models can be

computationally intensive (e.g., [18,19]). As risk-sensitive planning can require iterating through successive urban plans/designs (e.g., [89]; this special issue), the computation time of physics-based methods could be a limiting factor relative to other methods. This can be mitigated by using surrogate models or emulators, calibrating against physics-based simulations or real observations to provide computationally efficient, data-driven approximate solutions (e.g., [20]). While we use this article to outline the importance of physics-based models in advancing effective risk-sensitive planning decisions for future urban development, we also recognise that empirical and stochastic models can also make useful contributions to well-defined components of planning frameworks, such as probabilistic hazard assessment for building code calibration (e.g., [21]). In summary, by understanding the benefits and limitations of the methods outlined above and used below, risk to future communities can be mitigated by using the most appropriate models to simulate natural hazards and their impacts.

We adopt the United Nations Office for Disaster Risk Reduction's (UNDRR) definition of 'multi-hazard' to mean "(1) the selection of multiple major hazards that the country faces, and (2) the specific contexts where hazardous events may occur simultaneously, cascadingly or cumulatively over time, and taking into account the potential interrelated effects" [22]. Below, we primarily consider the first part of this definition at the urban scale (i.e., multiple hazards that do not occur coincidentally or dynamically interact). Specifically, in this study, we use physics-based models to simulate multiple independent natural hazards in a virtual urban testbed to elucidate the advantages and challenges of using these models for risk-sensitive urban planning. We simulate multiple natural hazard scenarios featuring earthquakes (Section 3), fluvial and pluvial flooding (Section 4), and debris flows (Section 5). All scenarios presented here are simulated in 'Tomorrowville', a virtual urban testbed introduced below in Section 2. In Section 6, we synthesise our results and reflect on the identification of potential multi-hazard events. Finally, we reflect on the challenges researchers/modellers, stakeholders, and city planners face in using physics-based models for risk-sensitive urban planning and decision making. We outline how the Tomorrow's Cities Decision Support Environment (TCDSE) design and implementation can limit these challenges.

2. Overview of Tomorrowville

Tomorrowville is a virtual urban testbed which has been designed to represent typical physical and socio-economic aspects of evolving cities in the Global South ([92]; this special issue). In this special issue, an interdisciplinary group of researchers use Tomorrowville as a platform to develop and test the Tomorrow's Cities Decision Support Environment ([89-91]; this special issue). In this work, we simulate multiple hazards in the present-day (i.e., initial) urban development configuration of Tomorrowville (denoted as TV0). More details on various configurations of Tomorrowville can be found in [92] (this special issue). The underlying landscape of Tomorrowville comprises a valley floor and terraced slopes that separate two high-elevation plateaux (Fig. 1). An active river channel is located at the base of the valley floor. During intense rainfall, ephemeral channels develop in incised valleys. Settlements are located on the eastern plateau and clustered in the central valley region. For the purpose of this analysis, we assume that the region is affected by three types of hazards: flooding, debris flows, and earthquakes.

The topographic domain of Tomorrowville is derived from a 2 m resolution digital surface model (DSM) of a ~6 km^2 section of the Kathmandu Valley (KTMV), derived from tri-stereo Pleiades satellite imagery. This area of the KTMV was selected to represent Tomorrowville due to several key considerations: principally, community engagement identified three natural hazards (earthquakes, flooding, and debris flows) that impact this area; this area is covered by a high-resolution digital elevation model (DEM) that can be used for high-resolution urban flooding and debris flow simulations; we have access to lithological/sedimentological data which can be used to determine model parameters. To assess the DEM's vertical accuracy, we coregister and compare the Tomorrowville

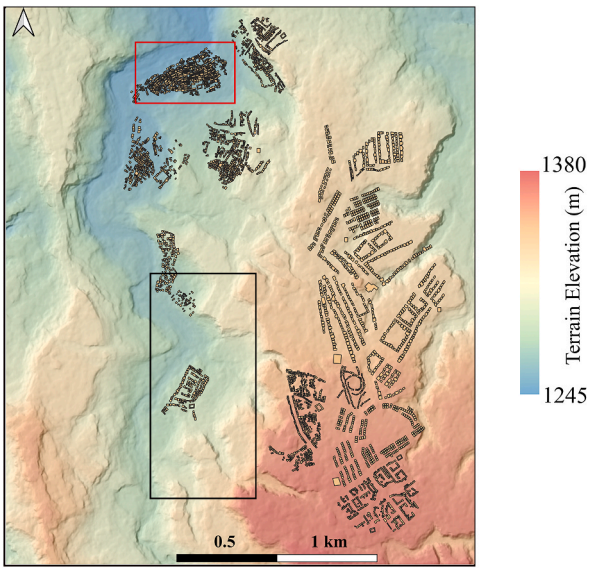

Fig. 1. Digital elevation model (DEM) of TV0 with boxes indicating the location of zoomed in Figures in Section 4 and Section 5.

elevation model to available ICESat (Ice, Cloud, and land Elevation Satellite)-2 altimetry data [23] over slopes less than 10°. The Normalised Median Absolute Deviation (NMAD) [24] and Root Mean Square Error (RMSE) between the two datasets were 0.46 m and 0.75 m, respectively. By comparison, the RMSE for globally available 30 m resolution DEM products commonly used for flood modelling, such as the Shuttle Radar Topography Mission (SRTM) or ALOS World 3D (AW3D30), is typically 5–10 m (e.g., [25]). Stochastic simulations that produce multiple topographic realisations using spatially correlated DEM errors are required to fully quantify the influence of DEM error on flow routing (e.g., [26,27]). Surface features (e.g., buildings and trees) present in the original KTMV DSM were removed using LAStools software for ground classification before the elevations corresponding to the building layout of TV0 were added. The inclusion of building elevations in Tomorrowville's DEM can influence the routing of hazardous flows through settlements (Section 4).

In the scenarios presented here, several assumptions were made in developing the physics-based models. For example, in a real landscape, model parameters would have to be calibrated and validated against observed historical events to ensure appropriate accuracy. In the absence of reliable historical data commonly used to calibrate the models, it would be essential to explicitly define the bands of uncertainty associated with uncalibrated models. Because of the nature of this research, where the models have been developed for a virtual urban testbed for demonstration purposes of the TCDSE concept, the calibration of model input parameters and source conditions and validation of model output against observations has not been carried out for Tomorrowville. Instead, this study presents comparative scenarios for each hazard, with scenario intensities selected to represent typical hazards that affect Global South cities (see below). These scenarios are subsequently used to demonstrate the importance of modelling multiple hazards and incorporating climate change projections when designing risk-sensitive future urban plans. For the TCDSE, various hazard scenarios would be simulated for each hazard to produce a database of dynamic intensity maps. These can be, in turn, used within the TCDSE's 'Physical Infrastructure Impact' module to assess impacts from natural hazards on the built environment, for instance, through appropriate fragility (i.e., the probability of various damage levels as a function of a hazard intensity measure) and consequence models (e.g., [89-91]; this special issue).

3. Earthquake hazard

Earthquakes produce damaging ground shaking, which globally has caused billions of dollars of economic losses and almost one million fatalities so far in this century (e.g., [28]). In earthquake-prone regions, understanding the potential for strong ground shaking is essential for the design of new structures and the performance assessment of existing structures and infrastructure components within the built environment. This has led to the development of a range of methods to assess seismic hazard (e.g., [29–31]). Seismic hazard analysis relies on two main components: (i) modelling potential rupture scenarios in the vicinity of the region of interest; and (ii) estimating the ground-motion properties (or local intensities) caused by a given scenario rupture. Compilations of ground-motion records from past earthquakes of different sizes across an area have led to a series of empirical GMMs – based on regression analysis – estimating the probability distributions of ground-motion intensity measures at a site, given an earthquake of a certain magnitude occurring at a nearby location. Specifically, these models relate the magnitude and style of a seismic event, the distance from the source, and other site-specific parameters (e.g., local soil properties) to the amplitude and other features (e.g., significant duration) of the expected shaking and its variability at a given target site (e.g., [17,32-33]). While providing a systematic and effective method for estimating ground-motion parameters, such ground-motion modelling suffers from several critical shortcomings. First, the paucity of high-magnitude/high-intensity recordings at small distances requires extrapolation of the models into the most important parts of the domain. The scarcity of instrumental recordings, particularly in the Global South where urban expansion is concentrated, often requires the import of GMMs into areas for which their efficacy is questionable and where validation is not always possible. Finally, nonlinear time-history analysis of engineered systems arguably represents the most advanced procedure for structural seismic performance assessment and fragility analysis (e.g., [34,35]). Such analysis procedures require reliable ground-motion time series to investigate structural response to dynamic loading. Generally, the input ground-motion time series for nonlinear structural analysis are selected (and eventually scaled) from a database of existing records to represent target seismic characteristics at a given location (e.g., [36]). As discussed above, the inherent scarcity or total absence of suitable recorded ground motions for some specific scenarios (e.g., large-magnitude strike-slip events recorded at close source-to-site distances) makes the use of alternative options unavoidable.

In particular, physics-based ground-motion simulation has emerged as a complementary and possibly alternative approach to empirical ground-motion modelling, addressing the abovementioned challenges [37]. This method utilises a representation of the earthquake source using dynamic or kinematic rupture models and solves the wave propagation equations to simulate the shaking time series at the surface of the Earth (e.g., [38–45]). These physics-based simulated ground motions can capture complex source features (such as spatially variable slip distributions, rise-time, and rupture velocities); path effects (geometric spreading and crustal damping); and site effects (wave propagation through basins and shallow site response), providing a valuable supplement to recorded ground motions. Hence, in the specific context of high-resolution hazard modelling for urban planning, physics-based ground-motion simulations can provide estimates of full ground-motion time series, enabling an improved assessment of the complete range of ground-motion features. Moreover, these waveforms can be coupled with advanced nonlinear structural models to perform nonlinear time-history analysis of buildings and infrastructure components and derive sophisticated, numerical models of structural fragility (e.g., [97]; this special issue). In this way, physics-based ground-motion simulations provide risk modellers and decision-makers with a scientifically rigorous basis for estimating the likely impacts of strong shaking at the scale of individual assets.

Below, we present simulations from physics-based and empirical GMMs to compare the advantages and limitations of these methods and to provide insight into how physics-based simulation can assist in urban planning and decision-making. We examine the potential of a physics-based set of earthquake simulations to expose some invariants of the shake distribution for a series of idealised

events around Tomorrowville. We demonstrate that the relative amplitude of local shaking is strongly constrained by the near-surface velocity structure and identify robust patterns of relative amplitudes of ground shaking that permit detailed estimations of spatial distributions of relative shaking amplitude regardless of the fault mechanism, locations, directivity or even magnitude of the event.

3.1. Model setup

3.1.1. Geological setting

We first construct a simple but reasonable velocity structure for the crust below our testbed area. 3D crustal models (often referred to as 'velocity models') provide the 3D domain over which the wave equation is solved. The crustal model provides the 3D variation of geophysical and geotechnical parameters required for wave propagation calculations. The principal parameters to describe the model are the P- and S-wave velocities, density, and anelastic attenuation — additional parameters are needed if nonlinearities are considered.

Tomorrowville, similarly to many areas slated for urban development, is located around a river channel, under which a deeper sedimentary layer is assumed. Soft sedimentary layers influence earthquake-induced ground motions (e.g., [44–47]); hence, their explicit consideration in the model is crucial. Fig. 2 presents the extent of the river channel within the wider basin, the location of Tomorrowville, and the shear-wave speed (V_s) for the entire simulation domain.

The depth-dependent velocity structure of the simulation domain, including density (ρ), the shear wave speed (V_s), primary-wave speed (V_p), and anelastic attenuation factors (Q_s and Q_p), is generated based on the values assumed for V_s at the surface for the river channel, basin interior, and basin exterior (see Table 1). We use Brocher [48] (equation 9) to relate V_p to V_s for the basin exterior region. Note that in the absence of site-specific data, the use of an empirical velocity model is essential to enable the estimation of ground motion using physics-based simulations. We assume that anelastic attenuation is given by $Q_s = V_s/20$ and $Q_p = 2Q_s$. In addition, we introduce some stochastic variability in the underlying crust by perturbing the velocity at each point, producing a fractal spatial correlation in the velocity structure. Currently, this perturbation has an arbitrary amplitude proportional to the velocity at any point but provides realistic spatial correlations consistent with observations in deep boreholes (e.g., [49]). These choices are unlikely to significantly alter the main conclusions of this paper.

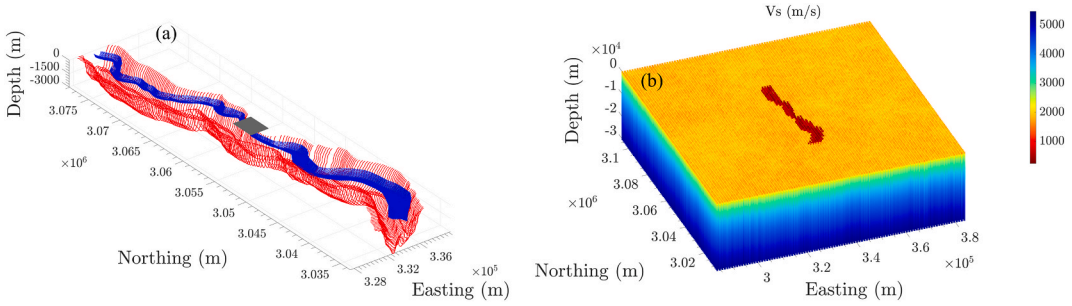

Fig. 2. (a) Geometry of the river basin sedimentary sequence (blue) and the deeper basin in which it is situated. The grey rectangle indicates the surface location of Tomorrowville within this basin. (b) Extent of the river channel and larger basin and the 3D distribution of shear-wave speed for the entire simulation domain.

Table 1
Velocity structure of the earthquake simulation domain.

River channel	Basin interior	Basin exterior
Mean V_s at the surface (μ) [m.s^{-1}]		
350	550	1800
V_s variation factor (δ)		
100	150	200
V_s profiles [m.s^{-1}]		
$\mu + \delta r + 15\sqrt{z}$	$\mu + \delta r + 15\sqrt{z}$	$\mu + \delta r + 20\sqrt{z}$
V_p profiles [m.s^{-1}]		
1.87 $\bullet V_s$	1.87 $\bullet V_s$	$V_p = a_0 + a_1 V_s - a_2 V_s^2 + a_3 V_s^3 - a_4 V_s^4$, with $a_0 = 940, a_1 = 2094.7, a_2 = 820.6, a_3 = 268.3, a_4 = 25.1$
Density profiles [10^3 kg m^{-3}]		
$(0.00174 \bullet V_p)^{0.25}$	$(0.00174 \bullet V_p)^{0.25}$	$(0.00174 \bullet V_p)^{0.25}$

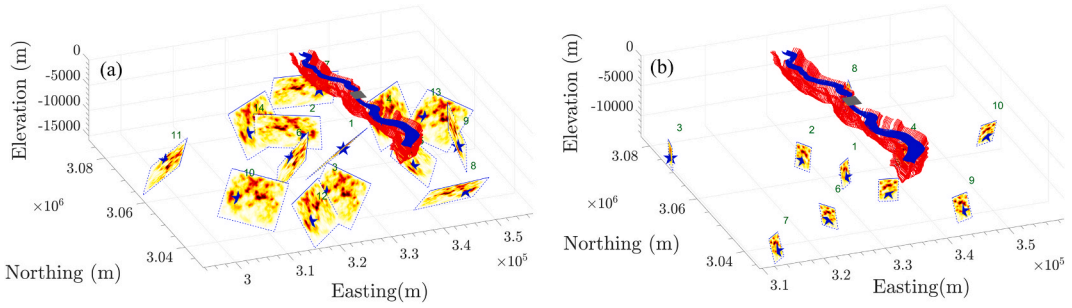

Fig. 3. Location and geometrical attributes of the M_w 6.0 (a) and 5.0 (b) scenarios. The stars show the rupture initiation points (i.e., hypocenters) on the rupture planes, and the coloured planes display the spatial distribution of the moment release as shown in Fig. 4.

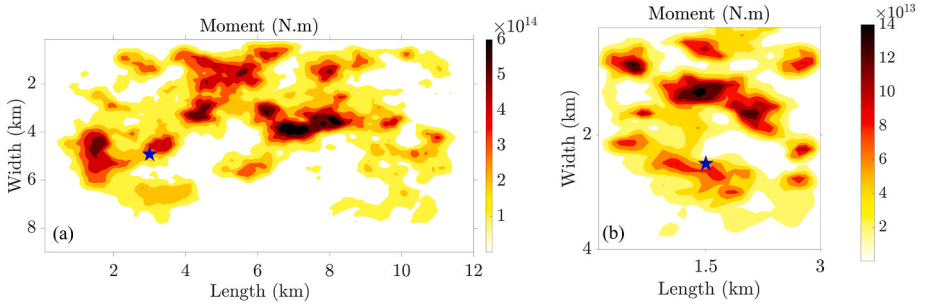

Fig. 4. Moment release in the kinematic rupture models generated for the considered Mw 6.0 (a) and 5.0 (b) scenarios.

3.1.2. Seismic sources

We now explore the shaking modelled across Tomorrowville due to different earthquake events. Here, we compute the shaking at every node of the surface of the computational domain so that we can compute the peak spectral accelerations at each point for each event. We simulate 14 $M_w = 6$ events, illustrated in Fig. 3a; and 10 $M_w = 5$ events, illustrated in Fig. 3b. As shown in Fig. 4, the slip distribution remains the same for each magnitude. Still, the strike, dip, rake and hypocentral depth vary, producing a wide range of expected source directivity for any location. The aim of considering these two sets was to scrutinise the effect of the underlying geological structure on the spatial ground-motion intensity measures for a range of modelled events. Two simulation cases (scenario EQ1 from the M_w 5.0 set and scenario EQ2 from the M_w 6.0 set) are used to assess the utility of physics-based ground-motion simulations for risk-informed urban planning (see Section 3.3). Kinematic rupture models for the considered scenarios in Fig. 4 are generated based on the model developed by [50,51]; in which the correlation between the slip, rise time, peak time and rupture velocity in the neighbouring sub-faults are considered based on a large ensemble of dynamic simulations. Fig. 4 presents the moment release across the rupture for the M_w 6.0 and M_w 5.0 scenario events.

3.1.3. Simulation methodology

Simulations are performed using the spectral element approach for solving the wave-propagation equations. The resulting ground motions at the surface of the domain are extracted using SPEED (SPectral Elements in Elastodynamics with Discontinuous Galerkin approach), an open-source package developed by [52]. Using the p- and h-adaptivity of the spectral element method, the solution to the wave propagation problem in a large domain can be found in a computationally efficient way by varying element size and spectral degrees. A critical factor in the numerical solution of the 3D wave equation with comprehensive physics is that the maximum frequency that can be modelled is a function of the model spatial resolution (i.e., grid spacing). Considering the minimum V_s of 250 m/s, the smallest element size of 200 m, and a spectral degree of 4 (to constrain the simulation from a computational cost perspective), the simulations are valid for vibration periods larger than 0.8 s. Given the domain size and the resolution of the simulation, small-scale topographic variation of the Tomorrowville region is neglected in our earthquake simulations.

3.2. Results

The simulation results are presented in Fig. 5 in terms of 5%-damped pseudo-spectral accelerations (pSAs) at the vibration period of 1.0 and 2.5 s. These periods can capture the medium- and long-period ground-motion amplitudes relevant for the physical-damage assessment of any mid- and high-rise buildings in Tomorrowville. The geometrical mean of the two horizontal ground-motion intensity measures is shown only for the Tomorrowville region. Fig. 5 shows that the soft sedimentary layer near the river channel and the basin interior amplify the ground shaking significantly for both M_w 6.0 (i.e., Fig. 5a-b) and M_w 5.0 (Fig. 5c and d) scenarios relative to the terraced slopes and upper plateau regions. It is noted that the event EQ1 of the M_w 5.0 ensemble is located exactly underneath the soft sedimentary basin. In contrast, the EQ2 event of the M_w 6.0 ensemble is located in the stiff basin exterior region with backward

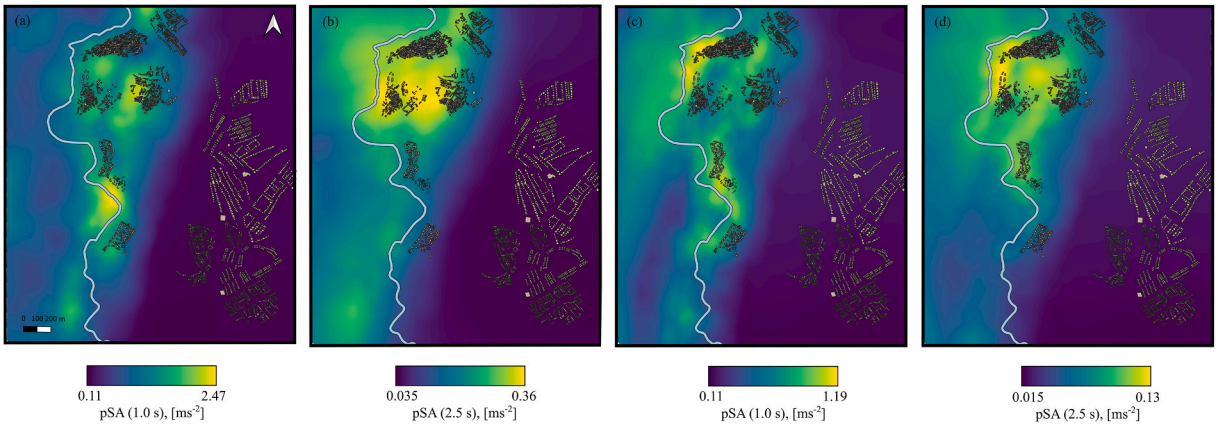

Fig. 5. Geometrical mean of the pSA(1.0 s) and pSA(2.5 s) for the M_w 6.0 EQ2 event (a-b) and M_w 5.0 EQ1 event (c-d).

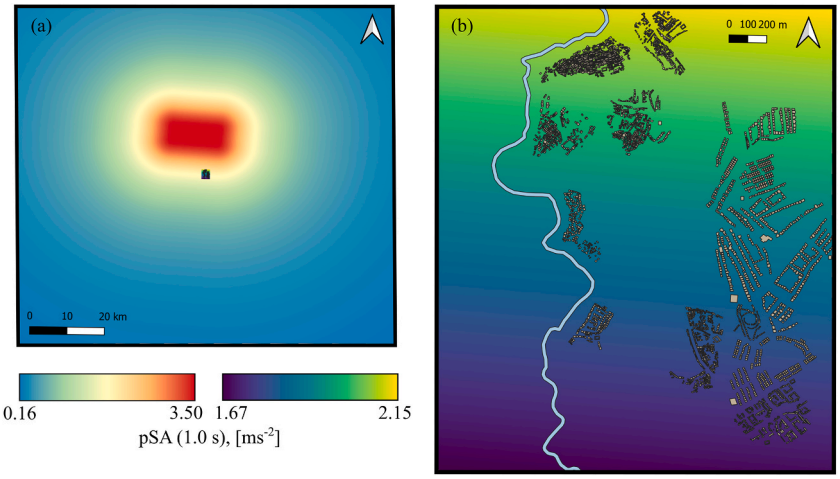

Fig. 6. Median of pSA(1.0 s) calculated based on an empirical ground motion model for M_w 6.0 EQ2 scenario Displayed for the full (100 × 100 km) empirical simulation domain (a) and zoomed in for Tomorrowville (b). Note that we overlay panel (b) on the empirical domain (a) to illustrate the location of TV0.

directivity towards the basin. Regardless of the rupture direction and energy content released by the two events, both result in large-amplitude high-duration motions in the basin region.

Fig. 6 presents the counterpart results from an empirical GMM (e.g., [53]), for the M_w 6.0 event EQ2 (median estimate). These results are presented in the Tomorrowville region as well as a 100 × 100 km extent to reveal the general trend in estimates from empirical models. It is noted that the empirical results are produced for a V_s 30 = 300 m/s which is the V_s 30 value in the basin and river channel region (with no variation due to the specific depth sampling considered in the adopted velocity model). The intensity measure estimates follow a general race-track pattern. These results, which are representative outputs of empirical models, do not reproduce the small-scale, site-specific spatial variation that can be simulated using physics-based models (Figs. 5 and 7).

Fig. 7 presents the median pSA(1.0 s) and pSA(2.5 s) maps calculated based on the 10 and 14 event realisations considered, respectively, for Mw 6.0 and Mw 5.0 scenarios. As shown, the spatial pattern of the median (and other percentiles not shown here for brevity) intensity honours the main geological features of the region (i.e., sedimentary basin), which cannot be adequately addressed by empirical models in a site-specific fashion (Fig. 6). [37] discusses the ongoing challenges in physics-based ground motion prediction, namely: continued validation against recorded earthquakes to demonstrate the predictive capability of such methods and most efficiently identify avenues for improvement; theoretical developments in source, path, and site modelling within ground motion simulation; the explicit consideration of modelling uncertainties.

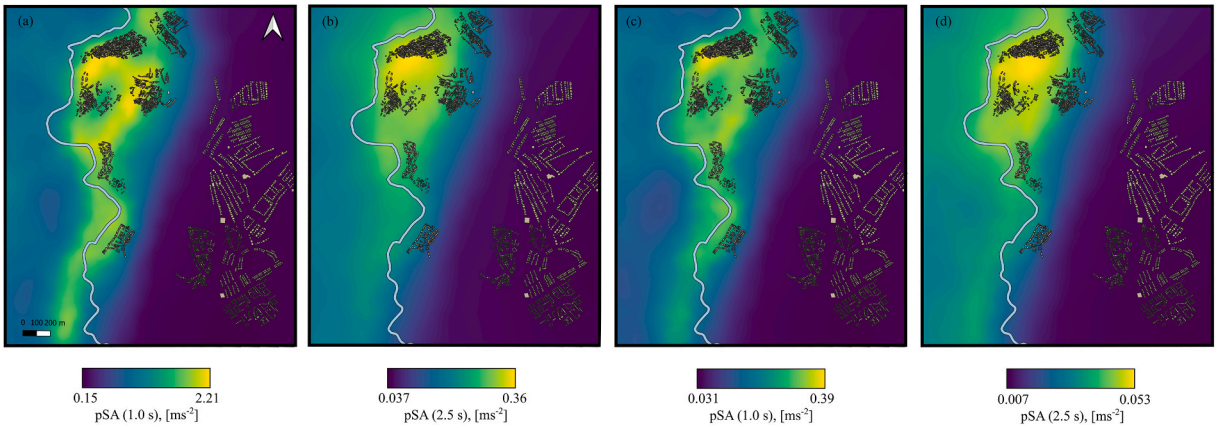

Fig. 7. Median of pSA(1.0 s) and pSA(2.5 s) calculated based on the 14 and 10 event realisations considered respectively for M_w 6.0 (a-b) and M_w 5.0 (c-d) scenarios.

4. Flooding hazard

4.1. Model setup

Flood events can be classified as fluvial, where the river banks are breached, pluvial, where rainfall runoff is the primary driver of the flood, or combined pluvial-fluvial floods. In urban areas, particularly where flash flooding occurs, it is essential to choose a numerical model which can consider the latter, i.e., combined pluvial-fluvial flood simulations (e.g., [54]). All flood simulation outputs presented here are in the form of inundation maps.

In this study, all flood simulations are generated using Caesar-Lisflood, a landscape evolution model (LEM) that combines the hydrological and surface flow model, Lisflood-FP [55], with the CAESAR landscape evolution model [56]. Lisflood-FP is a local inertial model derived from the full shallow water equations [55] that can model pluvial-fluvial flooding. It has been tested widely for use in rural and urban flood modelling, including as part of a European-wide flood study [57–59]. Neal et al. [60] showed that the Lisflood model can significantly reduce computational time while maintaining accuracy within 10% of full shallow water models in many applications, including flow over a floodplain. The model has some limitations for rapidly varied flows. For example, Lisflood cannot fully reproduce sharp wave fronts associated with dam break flows due to strong numerical diffusion. Using a fast flood model can allow us to simulate multiple hazard maps for different combinations of rainfall events and urban layouts while minimising computational effort. These hazard maps can then be used within the TCDSE to improve risk-informed urban planning and decision making. Another advantage of using a fast numerical scheme is that it can be used in combination with a high-resolution DEM. Although high-resolution DEMs increase computational time significantly, they can improve the representation of building footprints, river tributaries, and ephemeral channels and enhance flow routing accuracy through a domain [61]. Thus, the Caesar-Lisflood model was chosen for this study because it can be used to model both fluvial and pluvial flooding in combination with high-resolution DEMs in relatively short computational times, and it can also include sediment transport and erosion and deposition of the river channel (morphodynamics). Although no sediment dynamics are presented in the flood modelling in this paper, using Caesar-Lisflood allows scope for extending the research, with relative ease, to include interacting multi-hazard modelling, where sediment outputs and morphological changes generated from landslide and debris flow models, such as LaharFlow (see Section 5), can be incorporated into

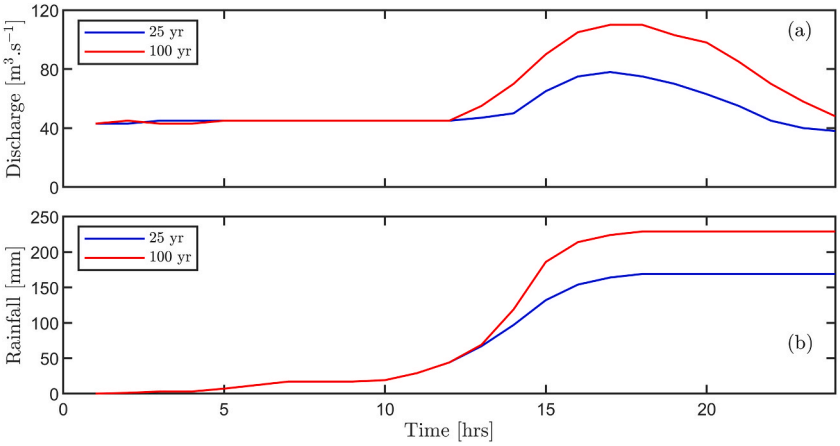

Fig. 8. (a) Discharge hydrograph (inlet and outlet) and (b) rainfall timeseries for two scenarios.

flood modelling. A detailed description of Caesar-Lisflood can be found in [56].

All flood scenarios discussed here are assumed to occur during a monsoon season. It is assumed that the soil is fully saturated by pre-monsoon rainfall so that, during the monsoon season, all rainfall becomes surface runoff. Although some runoff may be diverted to stormwater drainage systems, it is reasonable to assume that during the intense rainfall events presented in this study, typical urban drainage systems would reach capacity quickly, and the majority of rainfall would contribute to surface runoff. The TOPMODEL m parameter [62], required to calculate rainfall runoff in the Caesar-Lisflood model, is chosen to be small ($m = 0.003$) to represent this reactive rainfall-runoff system. In the absence of detailed information about land cover, sediment grain size, and bedforms, a uniform Manning's coefficient (which characterises any surface roughness that impacts water flow) of 0.04 ($m^{1/3}s^{-1}$) is used in all flood scenarios presented here [63]. In a real urban landscape, a spatially distributed Manning's coefficient could be calibrated to improve the accuracy of flow-routing through a domain with multiple land cover and channel types.

For the flood simulations, the discharge and rainfall time series are generated based on moderate to peak daily data based on recorded data from the Department of Hydrology and Meteorology, Nepal. In this way, the flood simulations are consistent with the Tomorrowville topography (extracted from the Kathmandu valley DEM, see Section 2). Three scenarios are presented: a fluvial flood event with a return interval of approximately 25 years (scenario F1), (discharge input from runoff in the upper catchment of the region), a fluvial-pluvial flood with an estimated recurrence interval of approximately 25 years (scenario F2), and a fluvial-pluvial flood with an estimated recurrence interval of 100 years (scenario F3). These events were chosen because analysis of projected future rainfall in Kathmandu has shown that a current 100-year return interval event could be equivalent to a 25-year event in the near future ([93]; this special issue). Therefore, using these two discharge hydrographs and rainfall time-series data allows us to explore the potential impact of climate change on future flooding hazard in Tomorrowville.

The initial conditions for all three scenarios are identical, with an initial water depth in the river reach only and no water on the floodplains. The discharge hydrographs shown in Fig. 8 are applied at the upstream boundary for all scenarios. For scenarios F2 and F3,

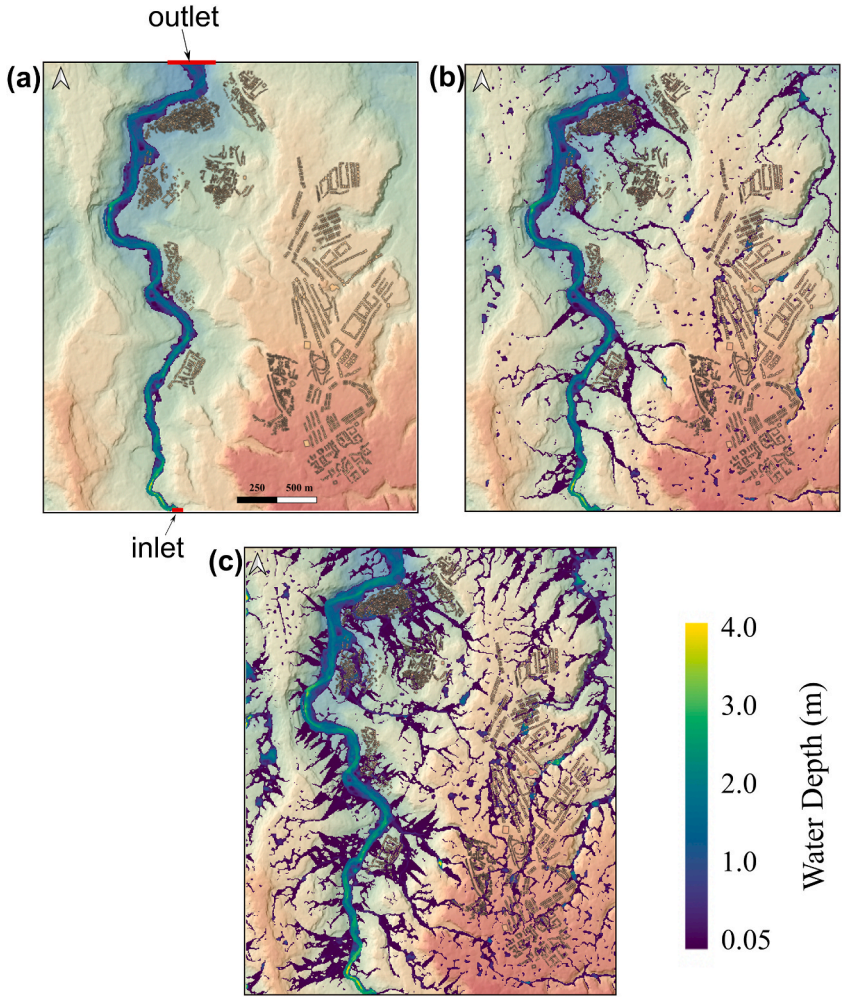

Fig. 9. Flood inundation maps for three scenarios: (a) fluvial flood; (b) 1-in-25 year pluvial-fluvial flood; (c) 1-in-100 year fluvial-pluvial flood. Inlet and outlet boundaries of the river are shown in Fig. 2(a) in red.

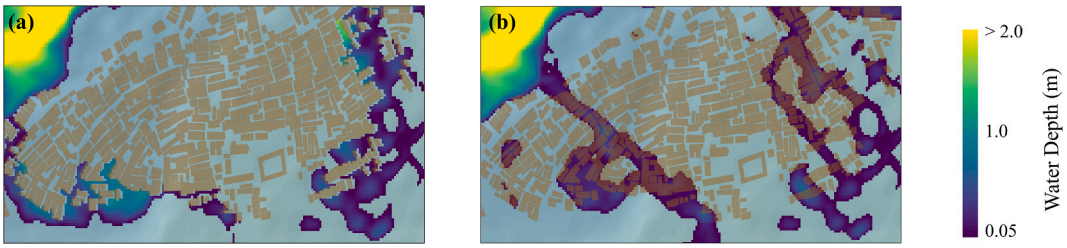

Fig. 10. Inundation depth at low lying residential area (outline shown in red in Fig. 1) for a 1-in-25 yr flood event for two different DEM scenarios: (a) TV0 building footprints are embedded into the DEM; and (b) TV0 building footprints are not embedded in the DEM.

as well as a discharge hydrograph, an hourly rainfall time series (mm/hr) of an estimated 1-in-25 year and 1-in-100 year rainfall event, respectively, is applied to every cell in the model domain (Fig. 8). Because of the size of the catchment (~6 km^2), we use a uniform rainfall distribution across the catchment. An open boundary condition is used at the outlet of the river (Fig. 9).

4.2. Results

Maps of maximum flood inundation for each of the three scenarios are shown in Fig. 9. For all scenarios, overbank flooding occurs along certain parts of the river, inundating a small number of buildings with up to 1–2 m of water. In Fig. 9a, where intense rainfall is neglected (F1), the flood inundation is confined to the region close to the river bank. Comparing the results of Fig. 9a–c, the flood inundation across the catchment increases when localised rainfall is considered. This highlights the need to use a combined fluvial/pluvial model to generate appropriate flood maps in urban regions prone to flash flooding. In addition, because of the terraced nature of the landscape, in Fig. 9b and c, the ephemeral rivers channel rainfall runoff to certain low-lying parts of the catchment. Not only does this increase the number of buildings in the catchment that are inundated, but runoff from the hills can results in some built-up areas becoming surrounded by flood depths in excess of 2 m. This is a crucial consideration in land-use planning because rainfall storms in Tomorrowville could result in people being isolated from essential services for the duration of the flood.

To test the effect of building footprints on the flow routing, we ran one additional scenario for the 1-in-25 year combined flood event using the 2 m DEM, which did not have TV0 building heights embedded. The results are shown in Fig. 10. For the overall catchment, the inundation pattern is similar. However, when we zoom in on the built-up areas (e.g., Fig. 10), we can see that the flood pattern is different, and the flood depths are greatly reduced when buildings are not considered (less than 0.4 m compared to depths more than 1 m–1.5 m when TV0 buildings are included). The presence of the building footprints in the DEM acts as an obstacle to the flow, causing it to be routed down certain streets and lanes between buildings. Because the flow cannot 'spread out' as it does in Fig. 10b, flow depths increase, potentially leading to increased flood damage (e.g., [97]; this special issue). This emphasises the importance of using physics-based flood simulations with high-resolution DEMs that include future urban footprints because the flood hazard is affected by both the urban landscape and the intensity of the rainfall/flood event. Note that the buildings are modelled as solid structures assuming that no flow enters the buildings. A model which allows buildings to be represented as porous or open structures may result in reduced flood depths, as the buildings provide additional volume for the flow to occupy (e.g., [64]). Therefore, models that neglect the flooding of building interiors are likely to overestimate flood depths in some locations. However, to the authors' knowledge, no open-source software with the ability to model building inundation is available at the time of writing, particularly for the scale of the urban zone being modelled in this study.

5. Debris flow hazard

Rainfall-driven debris flows and flash floods are energetic flows that often feature strong erosion and deposition (collectively referred to as morphodynamics). Their flow dynamics are inherently coupled to morphodynamics by: increasing or decreasing the mass of the flow through erosion or deposition of sediment, respectively; modifying the topography over which present and future flows are routed; and modifying the magnitude and form of basal drag. Debris flows damage buildings via inundation and by exerting dynamic forces on structures. When hydrodynamics forces are neglected, these forces are approximated by the hydrostatic pressure in the flow, allowing for the flow depth to be used as a proxy to estimate building damage resulting from debris flows, lahars, flash floods and other shallow overland flows (see [97]; this special issue; for a detailed discussion on appropriate fragility models).

5.1. Model setup

We simulate rainfall-driven debris flows using the LaharFlow dynamic hazard model [65,66]. Previously LaharFlow has been used to simulate two-phase, overland flows that feature strong morphodynamics, such as lahars, flash floods, and debris flows in arid-urban environments [65,67,68]. LaharFlow, as with many other models that simulate surface flows, utilises a shallow-layer formulation which assumes that the pressure distribution is hydrostatic and flow properties are vertically averaged. The model comprises a coupled system of partial differential equations that enforce conservation of mass and momentum in both the fluid and solid phases [66]. These equations are solved numerically over a 2 m resolution DEM of the target area in which building elevations are embedded. Note that in conserving mass in the fluid and solid phases separately, the model explicitly solves for the solids concentration of the flow, which is allowed to vary with morphodynamics. The model adopts well-established closures for morphodynamics: the erosive flux is

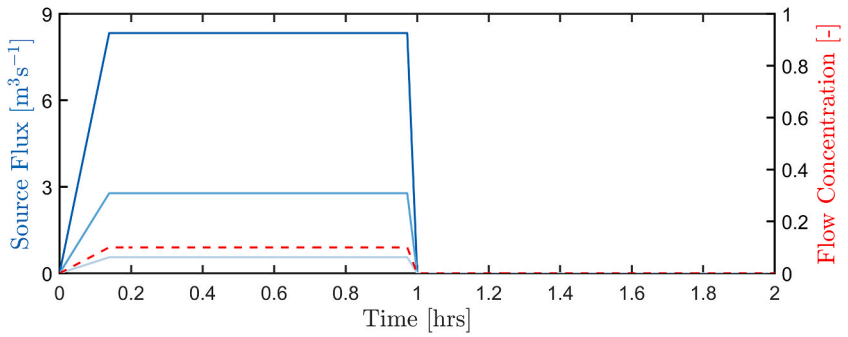

Fig. 11. Volumetric hydrographs used to initiate debris flows for low- (lightest blue), medium- (mid blue), and high-intensity (darkest blue) scenarios. The sediment concentration in the volumetric source is indicated by the dashed red line.

proportional to the excess Shields stress [69] and an erosion rate coefficient that is a function of the flow concentration. This smooth, monotonic function (hyperbolic tangent) accounts for the phenomenology that, for a given momentum flux, granular flows are more erosive than dilute flows. The depositional flux is calculated using a hindered settling law that accounts for the suppression of deposition as sediment concentration increases [70,71].

LaharFlow utilises a novel drag formulation to capture different basal stress modes present in flows across the entire range of sediment concentrations, from dilute, fluid-dominated flows to concentrated granular flows. Each of these limits utilises a widely adopted drag law: dilute flows use a Chézy drag formulation (e.g., [72]), whereas concentrated flows adopt a Coulomb law with a velocity-dependent friction coefficient [73]. A smooth, monotonic weighting function is used to determine the magnitude of basal drag for intermediate values of sediment concentration. Note that in the absence of morphodynamics at the dilute limit, the system of equations reduces to the familiar shallow water equations.

The source condition must be carefully chosen to ensure that the resulting debris flow is realistic. The domain is split into broadly three sub-domains that are approximately north-south oriented: a central river and low-relief zone separate two high-relief plateaux. Debris flows and other rainfall-driven overland flows require topographic focusing of surface runoff during high-intensity rainfall. The eastern plateau contains several valleys that are eroded by ephemeral channels that transport water and sediment to lower relief areas. We select a single valley (catchment area $\sim$0.2 km^2) as a location for the source of scenarios because the selected valley, and associated micro-catchment, is sufficiently large to focus a hazardous volume of surface runoff during intense rainfall, potentially inundating an area that could be deemed suitable for urban development. In contrast, smaller valleys/catchments are less likely to produce hazardous flows.

Debris flows are initiated by a volumetric flux distributed over a circular region with a radius of 50 m (location indicated in Fig. 12). This source area is chosen to be sufficiently large to ensure that flow in the source region respects the shallow-layer assumptions by preventing flow velocities and erosion in the source region from being unrealistically strong. We also ensure that flow is only introduced in the intended valley by selecting a source area smaller than the valley's width. The volumetric flux is calculated by multiplying the catchment area (0.2 km^2) by a time series hydrograph of rainfall intensity (m.s^{-1}). In our assumptions, we neglect infiltration and other water sinks during strong surface runoff promoted by the steep slopes in the source region.

We use peak rainfall intensities of 10, 50, and 150 mm h^{-1} for low-, medium-, and high-intensity debris flow scenarios, respectively. Note that the rainfall used to initiate debris flow scenarios is more intense (i.e., higher hourly rate) and of shorter duration than used for pluvial flooding scenarios. We find that, for the topography present in the target valley, short-duration, extreme intensity rainfall is required to erode and entrain non-negligible amounts of sediment necessary for these flows to be classified as debris flows. We base our source conditions on empirical intensity-duration thresholds for rainfall events that triggered recorded debris flows and landslides [74]. Despite the different hourly rainfall rates used for pluvial flooding and debris flow scenarios, the cumulative rainfall used to initiate these flow hazards is similar. As climate change will likely increase the frequency and intensity of extreme rainfall events in the case study area (e.g., [75]), considering a broad range of source rainfall intensities also allows us to account for a range of potential future climatic conditions in Tomorrowville. The source fluxes for these scenarios are summarised in Fig. 11. In each scenario, we impose the following source conditions:

1. The source flux linearly increases from 0 (m^3/s) to the maximum value over the first 500 s. The maximum flux is maintained for 50 min and then linearly removed over a period of 100 s. Linearly ramping the source up and down assists with model stability and limits the formation of artificial fronts in the flow, which sharp changes in the source flux can introduce. Note that in the absence of historical observations or flow data, the simple structure of an idealised hydrograph allows for a simpler interpretation of the resulting flow relative to more complex hydrographs.
2. The debris flow is initiated by setting the sediment concentration in the source flux to 10% solids (by mass). The addition of sediment allows for equilibrium between erosion and deposition to be established at earlier times. The addition of sediment to the source also accounts for sediment that is likely to be entrained whilst being routed from catchment to source. The sediment concentration is linearly ramped up to and down from its maximum value of 10%, as described for the volumetric source flux.

Table 2
Parameters used in LaharFlow simulations of debris flows.

Parameter	Value
Water density	1000 kgm^{-3}
Sediment density	2000 kgm^{-3}
Solids diameter	0.01 m
Bed porosity	0.35
Maximum packing fraction	0.65
Maximum erosion depth	1 m
Critical Shields Number	0.055
Fluid Erosion Rate	10^{-4}
Granular erosion rate	0.1
Chézy drag coefficient	0.04
Pouliquen Minimum Slope	0.1
Pouliquen Maximum Slope	0.4
Voellmy switch rate	3.0
Voellmy switch value	0.2

3. We continue running the simulation for an hour after the source is removed. This ensures that hazard maps include locations where the topography has focused the flow after removal of the source (typically furthest downstream).

The source condition is varied in all scenarios, and all other parameters are fixed (summarised in Table 2). Given that Tomorrowville is a virtual urban testbed, model parameters are selected to be consistent with values in the literature for similar magnitude debris flow events. The erosion parameters listed in Table 2 were tuned to yield erosion depths (tens of cm) consistent with direct measurements of erosion from debris flows [76]. Although stronger erosion has been observed from debris flows (>1 m), we limit erosion to a maximum depth of 1 m to ensure we are not capturing extreme behaviour. As discussed above, LaharFlow utilises a novel drag law that is a smooth function of solids concentration. Table 2 summarises the end member drag limits: a dimensionless Chézy drag coefficient of 0.04 lies within the range of calibrated field events studies (e.g., [77]). The minimum and maximum Pouliquen slope values correspond to the tangents of the angles at which a granular layer will begin and cease flowing, respectively (e.g., [78]). The Voellmy switch value can be interpreted as the sediment concentration (20%) at which granular effects begin dominating basal shear stress. Finally, the switch rate is tuned to control the sharpness of this transition.

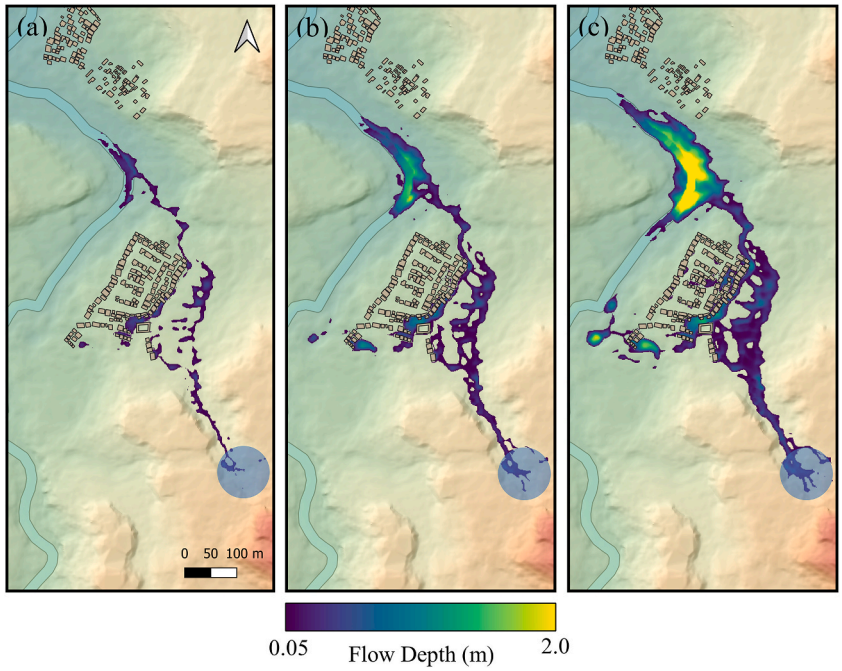

Fig. 12. Hazard maps displaying maximum depth of debris flow for low- (a), medium- (b), and high-intensity (c) scenarios. Note the location of these panels within Tomorrowville is indicated by a black rectangle in Fig. 1.

5.2. Results

We represent the hazard from debris flow scenarios using maps of maximum flow depth (see Fig. 12). In all scenarios, debris flows are routed through a single channel in the valley downstream of the source before spreading on the valley floor; partially inundate the settlement located on the valley floor; transport water and sediment into the river after following a channel to the north of the settlement. When simulating debris flow scenarios, we do not actively model fluvial transport of water/sediment that enters the river channel. Therefore, when debris flows enter the river channel, conservation of mass and momentum leads to the artificial development of expanding lakes (see Fig. 12). In reality, fluvial transport would likely prevent lake formation by advecting material downstream. Given that, in all simulations, these lakes never inundate any settlements or individual buildings, this assumption is unlikely to significantly impact debris flow routing through the urban settlement. Furthermore, we expect the effects from backward (i.e., upstream) propagation of the flow from these lakes to be limited, as these lakes mostly develop after the occurrence of maximum flow depth in the urban settlement. The strength of the source condition determines the severity of inundation in the settlement. Fig. 12 demonstrates that as the source intensity increases, the extent (i.e., number of assets affected) and depth of inundation increase. For higher intensity scenarios, an additional channel, located towards the southern extent of the settlement, becomes active, propagating the flow through the domain (Fig. 12b&c). In moderate to low scenarios, some ephemeral channels never become active. Given the large volume of material that can be deposited into the river for high-intensity scenarios, there is scope for considering multi-hazard interactions between fluvial flooding and debris flows (see below).

6. Discussion and conclusions

Our results demonstrate that physics-based models can be used to effectively simulate multiple independent hazards that impact an urban area. We now discuss the utility of these methods when developing risk-sensitive urban plans that consider multiple natural hazards. Physics-based models can produce high-resolution spatially distributed maps of hazard intensity for a range of scenarios. These can help decision makers identify regions of the landscape exposed to one or multiple hazards, from district level to individual buildings. When considering future urban development, the dynamic nature of the landscape and the hazards and the dynamic interactions between hazards and landscapes must be accounted for. For example, as the urban landscape evolves, the construction of new assets or the demolition of others can change the routing of flows (e.g., flood, debris flows, fire, etc.) through the landscape, thus changing the spatial intensity of flow hazards. This can be achieved using physics-based simulations only. We demonstrated this in the flood hazard modelling scenarios. When building footprints were incorporated into the DEM directly, the flood inundation increased in certain regions of Tomorrowville (Fig. 10). These features associated with the high-spatial-resolution mapping of building layouts are unlikely to be captured in empirical models that are not calibrated at this resolution. Physics-based models can also account for changes to flow behaviour and source conditions that arise from changes to surface runoff characteristics (e.g., from the construction of paved roads and new buildings). In addition, when considering future urban development, it is essential to account for the effects of climate change. Physics-based models can account for perturbations to parameters and source conditions likely to be caused by climate change. We demonstrated this in Section 4, where we incorporated rainfall projections from [93] into our flooding scenarios to demonstrate how climate change may alter flood hazard in Tomorrowville in the near future. This highlights the need to base future risk-sensitive urban plans on predicted rainfall events or projected climate scenarios and not only on return intervals produced from historical events. Physics-based models can be used to develop hazard maps for combinations of different physical urban layouts and hazard intensities when exploring potential future urban spaces.

The spatial correlations of hazards occur due to their dynamic behaviour and the physical characteristics of the domain. Most notably, settlements in the vicinity of the river channel are most vulnerable to future hazards due to: (a) overbanking of the river (fluvial flooding); (b) damage from debris flows and pluvial floods that are routed onto the valley floor; (c) maximum shaking from earthquakes occurs due to the soft sediments that surround the river channel and due to the basin geometry. Our results demonstrate that physics-based models can identify regions within Tomorrowville that are vulnerable to multiple independent hazards. Furthermore, using empirical GMMs as an example (Fig. 6), we demonstrate that empirical methods cannot resolve local-scale variations that contribute to the spatial correlation of hazards. It is important to identify multi-hazard interrelationships, as the cumulative impact of multiple interacting hazards can be greater than the sum of their individual impacts (e.g., [3,79]). This 'amplification' of impact can be caused by dynamic interactions between coincident hazards, and also by the accumulation of damage in the built environment from successive hazards (e.g., [80,97]). This study presented intensity maps for three independent hazards at the same physical locations. However, in a real landscape, interacting or cascading hazards could increase the exposure of the urban environment and vulnerability of its elements (e.g., including physical, social, and economic components); rapid urban expansion could further increase the susceptibility to certain multi-hazard interactions. For example, in a landscape like Tomorrowville, which is comprised of terraced slopes, a valley floor and upper plateau regions, the pressure on the land from urban expansion could lead to increased construction on steeper, unstable slopes. Earthquakes are known to trigger mass movements, including debris flows and landslides (e.g., [81]). Earthquakes may weaken hillslopes to the extent that they fail more readily when triggered by other mechanisms, such as intense rainfall (ibid.). Landslides, debris flows and floods can be considered as compound or cascading hazards, depending on the sequence of events (for an overview of possible hazard interrelationships, refer to [13,81,82]). In Section 5, we demonstrated that debris flows could potentially deposit sediment and water into the river. Under certain geographic conditions, this can alter river flooding by fully or partially damming rivers and increasing the volume of transported material (e.g., [83]).

The multi-hazard framework of [81] identifies four key sequential stages: (1) hazard identification and comparison; (2) hazard interactions; (3) hazard coincidence; (4) dynamic vulnerability. A challenge lies in establishing the existence or types of multi-hazard interactions using separate physics-based models that simulate different hazard scenarios. As the models used in this study are not

dynamically coupled, risk-sensitive plans will not account for the complex physical behaviour that occurs when hazards interact. Developing dynamically coupled models capable of simulating multiple interrelated hazards could provide a more complete representation of possible future multi-hazard events for use in risk-sensitive urban planning. In practice, examples of the integration of multi-hazard interrelationships remain limited (e.g., [84,85]). We have shown that independent physics-based hazard simulations, in combination with the literature and stakeholder knowledge, can be used to assist with the identification and location of multi-hazard prone regions. For Tomorrowville, we identify – at least qualitatively – potential multi-hazard interactions from simulations of individual hazards. In addition, for applying the TCDSE in an actual location, we also envisage a process of compiling and analysing a database of previous hazard and multi-hazard events from community knowledge, municipal government, risk management and media records. The resulting simulations should utilise DEMs that account for future urban designs (i.e., that represent future distributions of assets and populations). Several challenges exist in developing physics-based models to simulate natural hazards in an urban environment, including the identification of major hazards and their potential interactions, the choice of hazard intensity scenarios, the choice of model parameters, and the uncertainty associated with all of the above (e.g., [13]). However, using state-of-the-art physics-based models of multiple hazards can help to identify areas in a rapidly expanding urban landscape which are highly sensitive to multiple hazards. Understanding how different hazards interact with a landscape can help modellers, urban planners, policymakers and communities to identify areas more suitable for residential, industrial, leisure, and other land uses and for planning/designing future infrastructure systems.

Validation of physics-based models is essential to understand their accuracy and capability. In the case of a physics-based model for earthquake-induced ground motions, the appropriateness of input models describing the source rupture, 3D crustal structure, and shallow site conditions are complex and regionally varying. Hence, the accuracy of ground-motion simulations is region- and even site-specific. Furthermore, as ground-motion time series are complex transient signals, the power of simulations to adequately capture the relevant features of these signals varies depending on the specific focus of the analysis. Oberkampf et al. [86] discuss verification (i.e., assessing the accuracy of the solution of a computational model) and validation as a formal process for developing predictive capability in computational modelling. Bradley et al. [37] use those concepts to develop guidance on using earthquake-induced ground-motion simulation in engineering practice. Validation exercises involve testing simulations against observed data from past events. A generally favourable comparison of recorded and simulated intensities should provide confidence to stakeholders and decision-makers in using the proposed simulation method and its specific modelling components, particularly for future events.

When modelling natural hazards for risk-informed planning purposes, numerous sources of uncertainty must be understood and accounted for. Such modelling uncertainty is due to inaccuracies and idealisations made in the physics-based model formulations and the choices of source conditions and input parameters. While a detailed discussion of uncertainties in physics-based hazard simulations is beyond the scope of this work (and is also hazard- and method-dependent), we provide some general discussion and a few illustrative examples here. Specifically, three principal sources of modelling uncertainty in physics-based hazard models must be communicated to and considered by decision makers, including: errors in the physical domain; errors in the parameters contained within the governing equations; errors in the source/input conditions used to propagate hazards throughout the domain. Some of these issues can be addressed by thoroughly calibrating and validating the model using past events. However, it is impossible to calibrate and validate future projected hazards that depend on the urban layout (e.g., floods, mass movements, fires) that occur in regions that have yet to be developed. This is especially important for modelling the routing of hazardous flows since climate change and alterations to the physical environment caused by urbanisation will significantly affect modelling outputs, as discussed above. Physics-based models can simulate these physical changes by carefully selecting model parameters and source conditions based on future land use and climate projections. Moreover, different hazard models (and different modelling approaches/methods) will have different levels of uncertainty. Therefore, decision makers must be aware of, and adequately account for, those uncertainties when attempting to reduce risk in future urban environments. When using simulation-based risk-reduction frameworks, uncertainties—including those related to hazard intensities—should be propagated through to the relevant impact metrics. For instance, the simulation-based framework for earthquake risk-informed and people-centred decision making in future urban planning proposed in [6] explicitly accounts for uncertainties in the future projections of underlying variables (e.g., asset location and structural or non-structural features, building fragility, age and income profile of inhabitants). Monte Carlo sampling is extensively used to capture uncertainties in end-to-end calculations, from hazards to impacts and risk.

To illustrate some of these issues further, let us now consider uncertainties related to the domain of flow hazard simulations. A large source of error when simulating present-day flow hazards in urban environments is caused by artefacts in the DEM, such as: trees and vehicles, which provide obstacles to flow, and bridges over river channels, which can act as dams. These errors can be accounted for in present-day simulations by carefully processing the DEM to identify and remove these artefacts. However, the eventual layout of future urban environments is typically unknown precisely. Given that we have demonstrated the importance of incorporating future building layouts into the domains of flow simulations (see Section 4), decision-makers must recognise that perturbations to future urban plans can effectively alter future flooding hazard and therefore acts as a source of uncertainty in the risk-informed modelling process.

Some uncertainties associated with the limitations of individual physics-based models can be effectively communicated to stakeholders and decision-makers by leveraging a combination (ensemble) of different models for a given risk assessment. However, this approach requires an accepted protocol for ranking and aggregating models. The uncertainty associated with input parameters and source conditions can be accounted for in the planning process by simulating a range of scenarios co-produced with local stakeholders and decision-makers. For example, in the absence of historical flood maps from satellite imagery or maps developed as part of a post-disaster survey, communities can work with modellers to identify areas prone to flooding (e.g., [87]), as communities experiencing frequent natural hazards are known to have a wealth of local knowledge which can inform the modelling process [88]. Indeed, a key aspect of the TCDSE is to reduce risk in future cities by engaging with a broad spectrum of stakeholders throughout the planning stage

through a process of co-production [5].

In summary, we use a case study of a virtual urban testbed to highlight the importance of using physics-based models to simulate multiple natural hazards when designing risk-sensitive urban plans. We present simulations of independent earthquake, flood, and debris flow scenarios which we use to reflect on the process of integrating hazard models into risk-sensitive planning frameworks. We demonstrate that physics-based methods can be used to assist with the identification of urban areas that are vulnerable to multi-hazard events. We also show that including building elevations in high-resolution DEMs of future urban topography is necessary for planning that accounts for the routing of hazardous flows. We conclude by recommending that future risk-sensitive planning frameworks include physics-based models that can dynamically simulate coupled multi-hazard events that are identified through advanced modelling and co-production with local stakeholders.

Declaration of competing interest

The authors declare that they have no known competing financial interests or personal relationships that could have appeared to influence the work reported in this paper.

Data availability

Data will be made available on request.

Acknowledgements

The authors acknowledge funding from United Kingdon Research and Innovation (UKRI) Global Challenges Research Fund (GCRF) under grant NE/S009000/1, Tomorrow's Cities Hub.

Pleiades data were made available by CNES in the framework of the CEOS Working Group for Disasters. ©CNES (2019, 2020), and Airbus DS (2019, 2020), all rights reserved. Commercial uses forbidden. We thank J Elliott for negotiating access to Pleiades satellite imagery which was used to derive the Digital Elevation Model used in this study.

The authors thank Himanshu Agrawal for valuable discussions regarding the development of the seismic velocity model and the selection of seismic sources for the earthquake simulations in the paper, and Mark Woodhouse, Jake Langham and Andrew Hogg, for useful discussions regarding simulations of debris flows. We thank Gemma Cremen for providing constructive feedback on the study.

References

[1] C. Rosenzweig, W. Solecki, Hurricane Sandy and adaptation pathways in New York: lessons from a first-responder city, Global Environ. Change 28 (2014) 395–408, https://doi.org/https://doi.org/10.1016/j.gloenvcha.2014.05.003.
[2] D. Gu, Exposure and vulnerability to natural disasters for world's cities, United Nations Dep. Econ. Soc. Aff. (2019) 1–43.
[3] M.S. Kappes, M. Keiler, K. von Elverfeldt, T. Glade, Challenges of analyzing multi-hazard risk: a review, Nat. Hazards 64 (2012) 1925–1958, https://doi.org/10.1007/s11069-012-0294-2.
[4] G.D. Bathrellos, H.D. Skilodimou, K. Chousianitis, A.M. Youssef, B. Pradhan, Suitability estimation for urban development using multi-hazard assessment map, Sci. Total Environ. 575 (2017) 119–134, https://doi.org/https://doi.org/10.1016/j.scitotenv.2016.10.025.
[5] C. Galasso, J. Mccloskey, M. Pelling, M. Hope, C.J. Bean, G. Cremen, R. Guragain, U. Hancilar, J. Menoscal, K. Mwang, J. Phillips, D. Rush, H. Sinclair, International Journal of Disaster Risk Reduction Editorial. Risk-Based , Pro-poor Urban Design and Planning for Tomorrow ' S Cities, vol. 58, 2021.
[6] G. Cremen, C. Galasso, J. McCloskey, A simulation-based framework for earthquake risk-informed and people-centered decision making on future urban planning, Earth's Future 10 (2022), e2021EF002388, https://doi.org/10.1029/2021EF002388.
[7] G.D. Bathrellos, K. Gaki-Papanastassiou, H.D. Skilodimou, D. Papanastassiou, K.G. Chousianitis, Potential suitability for urban planning and industry development using natural hazard maps and geological-geomorphological parameters, Environ. Earth Sci. 66 (2012) 537–548, https://doi.org/10.1007/s12665-011-1263-x.
[8] C. Mesta, G. Cremen, C. Galasso, Urban growth modelling and social vulnerability assessment for a hazardous Kathmandu Valley, Sci. Rep. (2022) 1–16, https://doi.org/10.1038/s41598-022-09347-x, 2022 121. 12.
[9] G. Barrantes, Multi-hazard model for developing countries, Nat. Hazards 92 (2018) 1081–1095, https://doi.org/10.1007/S11069-018-3239-6/FIGURES/5.
[10] G. Barrantes, Multi-hazard model for developing countries, Nat. Hazards 92 (2018) 1081–1095, https://doi.org/10.1007/S11069-018-3239-6/FIGURES/5.
[11] U.N. Habitat, World Cities Report 2020: the Value of Sustainable Urbanization, 2020.
[12] C. Johnson, G. Jain, A. Lavell, Rethinking Urban Risk and Resettlement in the Global South, Rethink. Urban Risk Resettl, Glob. South, 2021, https://doi.org/10.14324/111.9781787358287.
[13] A. Tilloy, B.D. Malamud, H. Winter, A. Joly-Laugel, A review of quantification methodologies for multi-hazard interrelationships, Earth Sci. Rev. 196 (2019), 102881, https://doi.org/10.1016/J.EARSCIREV.2019.102881.
[14] D. Rickenmann, Empirical relationships for debris flows, Nat. Hazards 191 (19) (1999) 47–77, https://doi.org/10.1023/A:1008064220727, 1999.
[15] K. Usami, K. Ikehara, T. Kanamatsu, C.M. McHugh, Supercycle in great earthquake recurrence along the Japan Trench over the last 4000 years, Geosci. Lett. 5 (2018) 1–12, https://doi.org/10.1186/S40562-018-0110-2/FIGURES/4.
[16] F. Freddi, C. Galasso, G. Cremen, A. Dall'Asta, L. Di Sarno, A. Giaralis, F. Gutiérrez-Urzúa, C. Málaga-Chuquitaype, S.A. Mitoulis, C. Petrone, A. Sextos, L. Sousa, K. Tarbali, E. Tubaldi, J. Wardman, G. Woo, Innovations in earthquake risk reduction for resilience: recent advances and challenges, Int. J. Disaster Risk Reduc. 60 (2021), 102267, https://doi.org/10.1016/J.IJDRR.2021.102267.
[17] J. Douglas, B. Edwards, Recent and future developments in earthquake ground motion estimation, Earth Sci. Rev. 160 (2016) 203–219, https://doi.org/10.1016/J.EARSCIREV.2016.07.005.
[18] Y. Cui, E. Poyraz, K.B. Olsen, J. Zhou, K. Withers, S. Callaghan, J. Larkin, C. Guest, D. Choi, A. Chourasia, Z. Shi, S.M. Day, P.J. Maechling, T.H. Jordan, Physics-based seismic hazard analysis on petascale heterogeneous supercomputers, Int. Conf. High Perform. Comput. Networking, Storage Anal. SC. (2013), https://doi.org/10.1145/2503210.2503300.
[19] S.M. Vasconcellos, M. Kobiyama, F.S. Dagostin, C.W. Corseuil, V.S. Castiglio, Flood hazard mapping in Alluvial Fans with computational modeling, water resour, Manag 35 (2021) 1463–1478, https://doi.org/10.1007/S11269-021-02794-7/TABLES/2.
[20] A. Sarri, S. Guillas, F. Dias, Statistical emulation of a tsunami model for sensitivity analysis and uncertainty quantification, Nat. Hazards Earth Syst. Sci. 12 (2012) 2003–2018, https://doi.org/10.5194/NHESS-12-2003-2012.

[21] B.R. Ellingwood, Earthquake risk assessment of building structures, Reliab. Eng. Syst. Saf. 74 (2001) 251–262, https://doi.org/10.1016/S0951-8320(01)00105-3.
[22] UNDRR, Hazard Terminology, 2010. Https://Www.Undrr.Org/Terminology/Hazard. (n.d.).
[23] T.A. Neumann, A. Brenner, D. Hancock, J. Robbins, J. Saba, K. Harbeck, A. Gibbons, J. Lee, S.B. Luthcke, T. Rebold, ATLAS/ICESat-2 L2A Global Geolocated Photon Data, Version 3., Boulder, Color. USA. NASA Natl. Snow Ice Data Cent, Distrib. Act. Arch. Center, 2020, https://doi.org/10.5067/ATLAS/ATL03.005.
[24] J. Höhle, M. Höhle, Accuracy assessment of digital elevation models by means of robust statistical methods, ISPRS J. Photogrammetry Remote Sens. 64 (2009) 398–406, https://doi.org/10.1016/J.ISPRSJPRS.2009.02.003.
[25] E. Uuemaa, S. Ahi, B. Montibeller, M. Muru, A. Kmoch, Vertical Accuracy of Freely Available Global Digital Elevation Models (ASTER, AW3D30, MERIT, TanDE, 2010.
[26] T.A. Endreny, E.F. Wood, Representing elevation uncertainty in runoff modelling and flowpath mapping, Hydrol. Process. 15 (2001) 2223–2236 (https://doi).
[27] C.S. Watson, J. Carrivick, D. Quincey, An improved method to represent DEM uncertainty in glacial lake outburst flood propagation using stochastic simulations, J. Hydrol. 529 (2015) 1373–1389, https://doi.org/10.1016/J.JHYDROL.2015.08.046.
[28] EM-DAT the International Disaster Database, 2021. Https://Www.Emdat.Be/Index.Php.
[29] C.A. Cornell, Engineering seismic risk analysis, Bull. Seismol. Soc. Am. 58 (1968) 1583–1606, https://doi.org/10.1785/BSSA0580051583.
[30] S. Kramer, Geotechnical Earthquake Engineering, Pearson Education India, 1996.
[31] J. Baker, B. Bradley, P. Stafford, Seismic Hazard and Risk Analysis, Cambridge University Press, 2021.
[32] J. Douglas, H. Aochi, A survey of techniques for predicting earthquake ground motions for engineering purposes, Surv. Geophys. 29 (2008) 187–220, https://doi.org/10.1007/S10712-008-9046-Y/TABLES/8.
[33] J. Douglas, Ground Motion Prediction Equations 1964-2021, Www.Gmpe.Org, Uk, 2017.
[34] R. Gentile, C. Galasso, Simplicity versus accuracy trade-off in estimating seismic fragility of existing reinforced concrete buildings, Soil Dynam. Earthq. Eng. 144 (2021), 106678, https://doi.org/10.1016/J.SOILDYN.2021.106678.
[35] V. Silva, S. Akkar, J. Baker, P. Bazzurro, José M. Castro, H. Crowley, M. Dolsek, C. Galasso, S. Lagomarsino, R. Monteiro, D. Perrone, K. Pitilakis, D. Vamvatsikos, Current challenges and future trends in analytical fragility and vulnerability modeling, Earthq. Spectra 35 (2019) 1927–1952, https://doi.org/10.1193/042418EQS101O.
[36] I. Iervolino, C. Galasso, E. Cosenza, REXEL: computer aided record selection for code-based seismic structural analysis, Bull. Earthq. Eng. 82 (8) (2009) 339–362, https://doi.org/10.1007/S10518-009-9146-1, 2009.
[37] B.A. Bradley, D. Pettinga, J.W. Baker, J. Fraser, Guidance on the utilization of earthquake-induced ground motion simulations in engineering practice, Earthq. Spectra 33 (2017) 809–835, https://doi.org/10.1193/120216EQS219EP.
[38] D. Komatitsch, Q. Liu, J. Tromp, P. Süss, C. Stidham, J.H. Shaw, Simulations of ground motion in the los Angeles basin based upon the spectral-element method, Bull. Seismol. Soc. Am. 94 (2004) 187–206, https://doi.org/10.1785/0120030077.
[39] B.T. Aagaard, T.M. Brocher, D. Dolenc, D. Dreger, R.W. Graves, S. Harmsen, S. Hartzell, S. Larsen, M. Lou Zoback, Ground-motion modeling of the 1906 san Francisco earthquake, Part I: validation using the 1989 loma Prieta earthquake, Bull. Seismol. Soc. Am. 98 (2008) 989–1011, https://doi.org/10.1785/0120060409.
[40] M. Stupazzini, R. Paolucci, H. Igel, Near-fault earthquake ground-motion simulation in the grenoble valley by a high-performance spectral element code, Bull. Seismol. Soc. Am. 99 (2009) 286–301, https://doi.org/10.1785/0120080274.
[41] R.W. Graves, A. Pitarka, Broadband ground-motion simulation using a hybrid approach, Bull. Seismol. Soc. Am. 100 (2010) 2095–2123, https://doi.org/10.1785/0120100057.
[42] R. Taborda, J. Bielak, Ground-motion simulation and validation of the 2008 Chino hills, California, Earthquake Ground-motion simulation and validation of the 2008 Chino hills, California, earthquake, Bull. Seismol. Soc. Am. 103 (2013) 131–156, https://doi.org/10.1785/0120110325.
[43] R. Paolucci, I. Mazzieri, C. Smerzini, Anatomy of strong ground motion: near-source records and three-dimensional physics-based numerical simulations of the Mw 6.0 2012 May 29 Po Plain earthquake, Italy, Geophys, J. Intell. 203 (2015) 2001–2020, https://doi.org/10.1093/GJI/GGV405.
[44] D. Roten, K.B. Olsen, J.C. Pechmann, 3D simulations of M 7 earthquakes on the wasatch fault, Utah, Part II: broadband (0–10 Hz) ground motions and nonlinear soil behavior, Bull. Seismol. Soc. Am. 102 (2012) 2008–2030, https://doi.org/10.1785/0120110286.
[45] H.N.T. Razafindrakoto, B.A. Bradley, R.W. Graves, Broadband ground-motion simulation of the 2011 Mw 6.2 Christchurch, New Zealand, earthquake, Bull. Seismol. Soc. Am. 108 (2018) 2130–2147, https://doi.org/10.1785/0120170388.
[46] E. Maufroy, E. Chaljub, F. Hollender, J. Kristek, P. Moczo, P. Klin, E. Priolo, A. Iwaki, T. Iwata, V. Etienne, F. De Martin, N.P. Theodoulidis, M. Manakou, C. Guyonnet-Benaize, K. Pitilakis, P.Y. Bard, Earthquake ground motion in the Mygdonian basin, Greece: the E2VP verification and validation of 3D numerical simulation up to 4 hz, Bull. Seismol. Soc. Am. 105 (2015) 1398–1418, https://doi.org/10.1785/0120140228.
[47] C. Smerzini, K. Pitilakis, Seismic risk assessment at urban scale from 3D physics-based numerical modeling: the case of Thessaloniki, Bull. Earthq. Eng. 16 (2018) 2609–2631, https://doi.org/10.1007/S10518-017-0287-3/TABLES/4.
[48] T.M. Brocher, Empirical relations between elastic wavespeeds and density in the Earth's crust, Bull. Seismol. Soc. Am. 95 (2005) 2081–2092, https://doi.org/10.1785/0120050077.
[49] C.J. Bean, J. McCloskey, Power-law random behaviour of seismic reflectivity in boreholes and its relationship to crustal deformation models, Earth Planet Sci. Lett. 117 (1993) 423–429.
[50] P. Liu, R.J. Archuleta, S.H. Hartzell, Prediction of broadband ground-motion time histories: hybrid low/high- frequency method with correlated random source parameters, Bull. Seismol. Soc. Am. 96 (2006) 2118–2130, https://doi.org/10.1785/0120060036.
[51] J. Schmedes, R.J. Archuleta, D. Lavallée, A kinematic rupture model generator incorporating spatial interdependency of earthquake source parameters, Geophys. J. Int. 192 (2013) 1116–1131, https://doi.org/10.1093/GJI/GGS021.
[52] I. Mazzieri, M. Stupazzini, R. Guidotti, C. Smerzini, SPEED: SPectral Elements in Elastodynamics with Discontinuous Galerkin: a non-conforming approach for 3D multi-scale problems, Int. J. Numer. Methods Eng. 95 (2013) 991–1010, https://doi.org/10.1002/NME.4532.
[53] G. Lanzano, L. Luzi, F. Pacor, C. Felicetta, R. Puglia, S. Sgobba, M. D'Amico, A revised ground-motion prediction model for shallow crustal earthquakes in Italy, Bull. Seismol. Soc. Am. 109 (2019) 525–540, https://doi.org/10.1785/0120180210.
[54] M. Muthusamy, M.R. Casado, G. Salmoral, T. Irvine, P. Leinster, A remote sensing based integrated approach to quantify the impact of fluvial and pluvial flooding in an urban catchment, Rem. Sens. 11 (2019) 577, https://doi.org/10.3390/RS11050577, 11 (2019) 577.
[55] P.D. Bates, M.S. Horritt, T.J. Fewtrell, A simple inertial formulation of the shallow water equations for efficient two-dimensional flood inundation modelling, J. Hydrol. 387 (2010) 33–45, https://doi.org/10.1016/j.jhydrol.2010.03.027.
[56] T.J. Coulthard, J.C. Neal, P.D. Bates, J. Ramirez, G.A.M. de Almeida, G.R. Hancock, Integrating the LISFLOOD-FP 2D hydrodynamic model with the CAESAR model: implications for modelling landscape evolution, Earth Surf. Process. Landforms 38 (2013) 1897–1906, https://doi.org/10.1002/esp.3478.
[57] F. Dottori, L. Alfieri, A. Bianchi, J. Skoien, P. Salamon, A new dataset of river flood hazard maps for Europe and the Mediterranean Basin region, Earth Syst. Sci. Data Discuss. (2021), https://doi.org/10.5194/essd-2020-313.
[58] C.J. Feeney, R.C. Chiverrell, H.G. Smith, J.M. Hooke, J.R. Cooper, Modelling the decadal dynamics of reach-scale river channel evolution and floodplain turnover in CAESAR-Lisflood, Earth Surf. Process. Landforms 45 (2020) 1273–1291, https://doi.org/10.1002/ESP.4804.
[59] M.B. Malgwi, J.A. Ramirez, A. Zischg, M. Zimmermann, S. Schürmann, M. Keiler, A method to reconstruct flood scenarios using field interviews and hydrodynamic modelling: application to the 2017 Suleja and Tafa, Nigeria flood, Nat. Hazards 108 (2021) 1781–1805, https://doi.org/10.1007/s11069-021-04756-z.
[60] J. Neal, I. Villanueva, N. Wright, T. Willis, T. Fewtrell, P. Bates, How Much Physical Complexity Is Needed to Model Flood Inundation?, 2012, https://doi.org/10.1002/hyp.8339.
[61] M. Muthusamy, M.R. Casado, D. Butler, P. Leinster, Understanding the effects of Digital Elevation Model resolution in urban fluvial flood modelling, J. Hydrol. 596 (2021), 126088, https://doi.org/10.1016/J.JHYDROL.2021.126088.

[62] K.J. Beven, M.J. Kirkby, A physically based, variable contributing area model of basin hydrology, Hydrol. Sci. Bull. 24 (2009) 43–69, https://doi.org/10.1080/02626667909491834.
[63] V. Te Chow, Open Channel Hydraulics, McGraw-Hill, New York, 1959.
[64] D. Wüthrich, M. Pfister, I. Nistor, A.J. Schleiss, Experimental Study on the Hydrodynamic Impact of Tsunami-like Waves against Impervious Free-Standing Buildings, 2018, pp. 180–199, https://doi.org/10.1080/21664250.2018.1466676. Https://Doi.Org/10.1080/21664250.2018.1466676. 60.
[65] J. Phillips, M. Woodhouse, A. Hogg, J. Langham, The LaharFlow model for sediment flows and its application to huaycos in Chosica, strength, Capacit. Mitig. Huaico (Flash Flood) Impacts Peru (2018) 41–43, https://doi.org/10.1186/2191-5040-2-2.
[66] J. Langham, M.J. Woodhouse, A.J. Hogg, J.C. Phillips, Linear stability of shallow morphodynamic flows, J. Fluid Mech. 916 (2021) A31, https://doi.org/10.1017/jfm.2021.235.
[67] P. Tierz, M.J. Woodhouse, J.C. Phillips, L. Sandri, J. Selva, W. Marzocchi, H.M. Odbert, A framework for probabilistic multi-hazard assessment of rain-triggered lahars using bayesian belief networks, Front. Earth Sci. 5 (2017) 1–23, https://doi.org/10.3389/feart.2017.00073.
[68] A.J. Hogg, Predicting huaycos and lahars: physical models, mathematics and uncertainty, strength, Capacit. Mitig. Huaico (Flash Flood) Impacts Peru (2018) 25–27 (accessed March 24, 2022), http://repositorio.ingemmet.gob.pe.
[69] E. Meyer-Peter, R. Müller, Formulas for bed-load transport, 2nd Meet, Int. Assoc. Hydraul. Res. Int. Assoc. Hydraul. Res. (1948).
[70] R. Soulsby, Dynamics of Marine Sands, Thomas Telford Publishing, 1997 https://doi.org/902 10.1680/doms.25844.
[71] J.F. Richardson, W.N. Zaki, Sedimentation and fluidisation: Part I, Chem. Eng. Res. Des. 75 (1954) S82–S100, https://doi.org/10.1016/s0263-8762(97)80006-8.
[72] A.I. Shalaby, Fluid Mechanics for Civil and Environmental Engineers, CRC Press, 2018.
[73] Y. Forterre, O. Pouliquen, Flows of dense granular media, Annu. Rev. Fluid Mech. 40 (2008) 1–24, https://doi.org/10.1146/annurev.fluid.40.111406.102142.
[74] F. Guzzetti, S. Peruccacci, M. Rossi, C.P. Stark, The rainfall intensity-duration control of shallow landslides and debris flows: an update, Landslides 5 (2008) 3–17, https://doi.org/10.1007/s10346-007-0112-1.
[75] M.M. Sheikh, N. Manzoor, J. Ashraf, M. Adnan, D. Collins, S. Hameed, M.J. Manton, A.U. Ahmed, S.K. Baidya, H.P. Borgaonkar, N. Islam, D. Jayasinghearachchi, D.R. Kothawale, K.H.M.S. Premalal, J.V. Revadekar, M.L. Shrestha, Trends in extreme daily rainfall and temperature indices over South Asia, Int. J. Climatol. 35 (2015) 1625–1637, https://doi.org/10.1002/JOC.4081.
[76] C. Berger, B.W. McArdell, F. Schlunegger, Direct measurement of channel erosion by debris flows, Illgraben, Switzerland, J. Geophys. Res. Earth Surf. 116 (2011) 1–18, https://doi.org/10.1029/2010JF001722.
[77] D. Rickenmann, D. Laigle, B.W. McArdell, J. Hübl, Comparison of 2D debris-flow simulation models with field events, Comput. Geosci. 10 (2006) 241–264, https://doi.org/10.1007/s10596-005-9021-3.
[78] O. Pouliquen, Y. Forterre, Friction law for dense granular flows: application to the motion of a mass down a rough inclined plane, J. Fluid Mech. 453 (2002) 133–151, https://doi.org/10.1017/S0022112001006796.
[79] S. Terzi, S. Torresan, S. Schneiderbauer, A. Critto, M. Zebisch, A. Marcomini, Multi-risk assessment in mountain regions: a review of modelling approaches for climate change adaptation, J. Environ. Manag. 232 (2019) 759–771, https://doi.org/10.1016/J.JENVMAN.2018.11.100.
[80] G. Ganesh Prasad, S. Banerjee, The impact of flood-induced scour on seismic fragility characteristics of bridges, J. Earthq. Eng. 17 (2013) 803–828, https://doi.org/10.1080/13632469.2013.771593.
[81] J.C. Gill, B.D. Malamud, Reviewing and visualizing the interactions of natural hazards, Rev. Geophys. 52 (2014) 680–722, https://doi.org/10.1002/2013RG000445.
[82] S. De Angeli, B.D. Malamud, L. Rossi, F.E. Taylor, E. Trasforini, R. Rudari, A multi-hazard framework for spatial-temporal impact analysis, Int. J. Disaster Risk Reduc. (2022), 102829 https://doi.org/https://doi.org/10.1016/j.ijdrr.2022.102829.
[83] J.E. Costa, R.L. Schuster, The formation and failure of natural dams, Geol. Soc. Am. Bull. (1988) 1054–1068, accessed February 25, 2022, https://pubs.geoscienceworld.org/gsa/gsabulletin/article/100/7/1054/182167/The-formation-and-failure-of-natural-dams?casa_token=1wcDhs3dF9AAAAAA:Whtbg68AJVAxkK17qrBsZZ3YLbHtN5Dkd_GR0bXWMor5qcXgnZdG4URTklUMrYEzqpjJxw.
[84] N. Komendantova, R. Mrzyglocki, A. Mignan, B. Khazai, F. Wenzel, A. Patt, K. Fleming, Multi-hazard and multi-risk decision-support tools as a part of participatory risk governance: feedback from civil protection stakeholders, Int. J. Disaster Risk Reduc. 8 (2014) 50–67, https://doi.org/10.1016/J.IJDRR.2013.12.006.
[85] G. Cremen, C. Galasso, J. McCloskey, Modelling and quantifying tomorrow's risks from natural hazards, Sci. Total Environ. 817 (2022), 152552, https://doi.org/10.1016/J.SCITOTENV.2021.152552.
[86] W.L. Oberkampf, T.G. Trucano, C. Hirsch, Verification, validation, and predictive capability in computational engineering and physics, Appl. Mech. Rev. 57 (2004), https://doi.org/10.1115/1.1767847.
[87] J. Mulligan, V. Bukachi, R. Gregoriou, N. Venn, D. Ker-Reid, A. Travers, J. Benard, L.O. Olang, Participatory flood modelling for negotiation and planning in urban informal settlements, Proc. Inst. Civ. Eng. Eng. Sustain. 172 (2019) 354–371, https://doi.org/10.1680/JENSU.17.00020/ASSET/IMAGES/SMALL/JENSU172-0354-F9.GIF.
[88] R. Šakić Trogrlić, M. Duncan, G. Wright, M. van den Homberg, A. Adeloye, F. Mwale, C. McQuistan, External stakeholders' attitudes towards and engagement with local knowledge in disaster risk reduction: are we only paying lip service? Int. J. Disaster Risk Reduc. 58 (2021), 102196 https://doi.org/https://doi.org/10.1016/j.ijdrr.2021.102196.

Special issue references

[89] G. Cremen, et al., A state-of-the-art environment for supporting risk-sensitive decisions on urbanisation in tomorrow's cities, international journal of disaster risk reduction, International Journal of Disaster Risk Reduction under rev (2022).
[90] E. Menteşe, R. Gentile, G. Cremen, et al., Risk-informed urbanisation scenario development through interdisciplinarity and GIS-based spatial data generation process, International Journal of Disaster Risk Reduction under rev (2022).
[91] M.E. Filippi, et al., Interdisciplinarity in practice: reflections from early career researchers developing a risk-informed decision support environment for Tomorrow's Cities, International Journal of Disaster Risk Reduction under rev (2022).
[92] R. Gentile, G. Cremen, C. Galasso, et al., Scoring, selecting, and developing physical impact models for multi-hazard risk assessment, Int. J. Disaster Risk Reduc. (2022).
[93] D. Shrestha, D.B. Basnyat, J. Gyawali, et al., Rainfall extremes under future climate change with implications for urban flood risk in Kathmandu, Nepal. International journal of disaster risk reduction, International Journal of Disaster Risk Reduction under rev (2022).